This is the Pre-Published Version.

W.K. Cheung, Y. Zeng, S. Lin, X. Huang (2023) *Modelling Carbon Monoxide Transport and Hazard from Smouldering for Building Fire Safety Design Analysis*, **Fire Safety Journal**, 140, 103895. https://doi.org/10.1016/j.firesaf.2023.103895

Modelling Carbon Monoxide Transport and Hazard from Smouldering for Building Fire Safety Design Analysis

Wai Kit Cheung[a], Yanfu Zeng[a], Shaorun Lin[a,b], Xinyan Huang[a,*]

[a]*Research Centre for Fire Safety Engineering, Department of Building Environment and Energy Engineering, The Hong Kong Polytechnic University, Kowloon, Hong Kong*

[b]*Department of Mechanical Engineering, University of California, Berkely, CA, USA*

*Corresponding to xy.huang@polyu.edu.hk (X. Huang)

Abstract: Smouldering produces massive toxic smoke and carbon monoxide (CO) that is responsible for the majority of fire deaths, but current building fire safety design rarely considers smouldering hazards. This work investigates the transport and hazards of CO from smouldering fire for the building performance-based design practice. The numerical model is firstly validated by reproducing two flat-scale fire experiments, revealing the characteristic surface temperature and CO yield of smouldering sources. The smouldering fire scenario is then designed in an atrium to review the evolution of CO concentration and its associated Available Safe Egress Time (ASET). Results show that a smouldering fire of the same burning rate as a flaming fire not only can provide a similar ASET, but also present a greater threat to occupants and rescue teams by forming a cold layer of lethal CO on the ground. Hence, the smouldering fire scenarios and their CO hazards should be considered in the performance-based design of building fire safety. Simulations also reveal that the smouldering fire can be more dangerous as the atrium height decreases, and ceiling ventilation is particularly effective in extracting CO emissions from smouldering fires.

Keywords: *Smouldering fire; Toxic Smoke; Fire performance; Simulation; Safe Egress Time.*

1. Introduction

The main causes of deaths and injuries from fire accidents are overwhelming toxic gases, rather than the extreme heat from flame [1]. According to UK fire statistics, 63% of fatalities from fires were affected by toxic gases and smoke in 2021 [2]. Carbon Monoxide (CO) is the most lethal species among them because it blocks the absorption of oxygen by the blood and cannot be filtered by a mask. Excessive inhalation of CO may cause headaches, dizziness, nausea, and even death [3–5]. In a smouldering fire event, because it has no flame to burn out CO, the emission of CO could be much higher than in a flaming fire. Therefore, the CO emissions from smoky smouldering fires significantly threaten the life safety of the residents and firefighters. Besides, it is important to note that the smouldering dominated fires are more than we commonly expected, which could be confirmed by firefighters. For example, recent fire incidents in HK World Trade Centre and mini storage did not show

intense hot flame or heat release, but they generated massive smouldering smoke, causing many casualties (Fig. 1). Thus, building fire safety design should not ignore the hazards of smouldering fire.

Fig. 1. (a) Smoky fire in Hong Kong World Trade Centre, 2021; and (b) mini-storage fire in Hong Kong Amoycan Industrial Centre, 2016.

Performance-based design (PBD), as a scientific-based approach, has been widely adopted in the fire safety design of buildings [6,7]. By designing the typical and worst possible fire scenarios, fire modelling analysis is used to evaluate whether the fire protection provisions of the building, such as smoke management and fire compartmentation, are enough to protect the life safety of the occupants during the fire events. In current PBD practices, the fire scenarios of the building are designed by considering the maximum fire load, material property, possible ignition positions, etc. Based on the designed (flaming) fire scenarios, typically by a fire heat release rate (HRR), gas temperature, CO concentration, and smoke visibility are assessed by fire modelling to check whether or when the building will reach untenable conditions [8]. British Standard PD7974-6 suggests an 800 ppm to 1,200 ppm as a tenability limit of CO concentration in a fire scene. Exposed to such a CO concentration, occupants only have about 5 minutes before the toxic product impairs their capability of evacuation [9].

The performance of building fire safety is often defined by the available safe egress time (ASET) when one of the criteria first reaches the tenability limit at a predefined smoke clear height (e.g., 2 m). In most of the design cases, the HRR curves of flaming fires are defined by the growth rate and the peak value. Such a setting more or less implies that the heat release and hot gases from flame are the primary hazards in the fire. However, in most cases, the smoke visibility (caused by flame soot yield) rather than the temperature reaches the tenability limit first. Moreover, the critical CO concentration rarely reaches the defined limits in current design practices, although CO from flaming fires is often modelled in design and research [10,11]. This is opposite to the fire injury statistics, where toxic fire gases are the primary hazardous factor [2,5,12].

On the other hand, the fire smoke from burning common materials, e.g., wood, plastics, and fibre, include not only the soot particles from the flame but also massive pyrolysis and smouldering gases directly from the fuel surface. These pyrolysis and smouldering gases are not directly related to the flame HRR. For example, the smouldering of a few cigarettes can create a smoky environment and a

high CO concentration, while the burning HRR is negligible. A large flame not only helps burn out CO from pyrolysis and smouldering, but also drives smoke and CO to the ceilings due to the large buoyancy effect [13–15]. However, for the smouldering fire, all released CO will stay inside the built environment, particularly near the ground due to its low temperature. Therefore, using the HRR to define the fire scenarios could significantly overlook the hazards of smouldering fire and CO emissions [3,5,12].

Since the 1970s, several full-scale fire experiments have been done to analyse the toxic gases from smouldering fires. For example, Bukowski et al. [16] measured the CO and CO_2 concentrations from the smouldering cotton mattresses and cotton chairs in a typical house. The smouldering fuel burning rate and CO concentration were reported in a single room, an apartment, and a mobile home with different ventilation conditions [17–19]. Recent studies showed that the CO/CO_2 of smouldering fire ranged from 0.1 to 0.7 [20–22]. Only a limited number of numerical analyses on the emission of smouldering fire are available. For example, Saidi et al. [23] simulated packed beds of smouldering cigarettes and cellulose and analysed the velocity, temperature, and gas concentration profiles. So far, little work has identified the hazard of smouldering fire for the building fire safety design.

This work aims to investigate the CO transportation and hazard from the smouldering fire inside a built environment. The validation of the surrogate numerical model is first conducted by reproducing the CO profiles of full-scale smouldering experiments in the literature. Then, the model further quantifies the CO concentration profile for smouldering fires in the atrium and the associated Available Safe Egress Time (ASET). Finally, typical flaming and smouldering fire scenarios are compared to assess whether smouldering hazard is underestimated under various building and fire design conditions.

2. Flaming vs. Smouldering Fires and Emissions

Once heated, the hydrocarbon fuel decomposes to the char and releases a large number of pyrolysis gases, e.g., CH_4, CO, CO_2, H_2O, and HCN. Overall, the pyrolysis gases are flammable that can sustain a flame, and once burnt, the main products are H_2O and CO_2 (Fig. 2a). Under a good oxygen supply, most of the CO generated from the pyrolysis is further burnt in flame, so the mass yield or emission factor of CO is generally no more than 0.1 g/g [24].

On the other hand, smouldering combustion is the slow, low-temperature, and flameless burning of a solid fuel that occurs on the fuel surface [25,26]. Many common solid fuels or materials can smoulder, such as cigarettes, wood, cotton, fabrics, plastic foams, etc. In a smouldering fire (Fig. 2b), CO and other toxic gases released from the pyrolysis and char-oxidation processes will not be burnt in flame but will remain in the air. Thus, the emission factor of CO in a smouldering fire can increase to 0.2-0.3 g/g [21].

Despite the massive toxic gas production from smouldering fires, only flaming fires are considered as the design fire scenarios, often represented by a flaming fire HRR curve. One possible reason is that flaming fire could develop rapidly, showing a quick smoke spreading and temperature increase and a more direct threat to human beings.

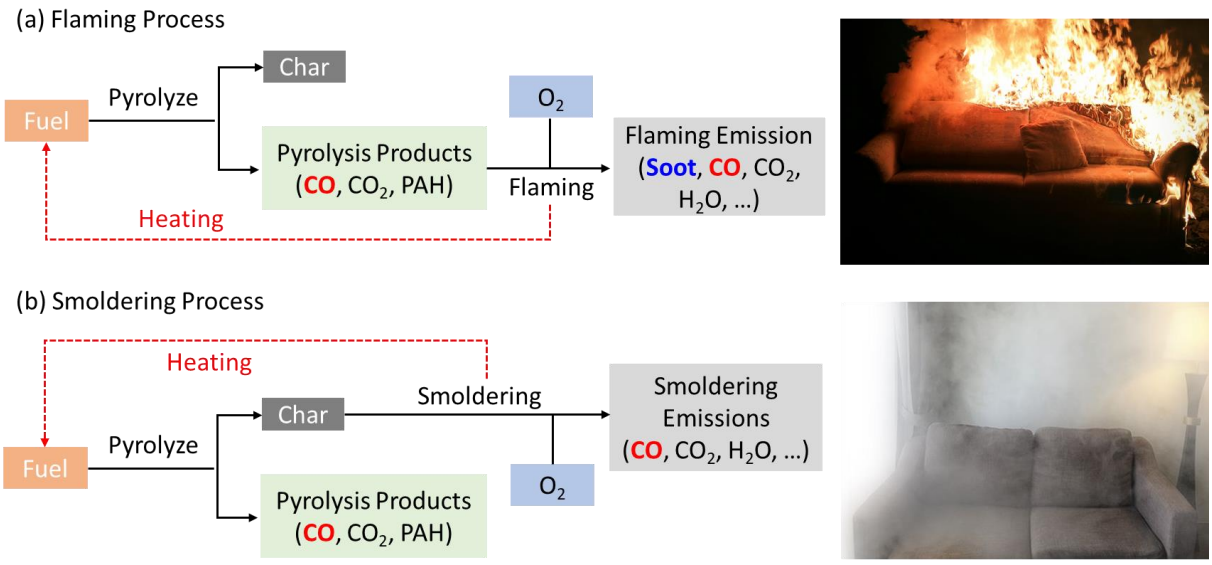

Fig. 2. Chemistry schematic diagrams and typical fire phenomena of (a) the flaming process; and (b) the smouldering process.

However, a smouldering fire can be more hazardous and lead to severe consequences. Except for the highly toxic emission, the designed sprinkler and fire detection systems are insensitive to the smouldering fire due to the low temperature of the burning surface and generated plume [27]. Many fire casualties occur when the occupants are slowly poisoned by the increasing CO concentration [3,5,12]. Additionally, a smouldering fire could also last for a much longer time compared to a flaming fire. A mini-storage fire in Hong Kong (Fig. 1b) smouldered for 108 hours, as firefighters could not control it effectively without targeting distinguished fire sources. Therefore, a better consideration of smouldering fire during the design stage should be provided.

3. Methodology

Setting appropriate inputs is crucial to the reliability and accuracy of a fire model. While the parameters of simulating a flaming fire, e.g., soot yield and burning surface temperature, have been validated by many research works [28], some properties which are important to model the smouldering fire remain unclear. Herein, two full-scale smouldering fire experiments in the late 1970s are first reproduced to calibrate the model settings: one is in a single enclosed room by Quintiere *et al.* [19], and another is in an apartment by Bukowski [17]. These experiments measured the smouldering mass-loss rate (or the fuel burning rate) during the experiments and CO concentrations at different locations.

For the model calibration, we conduct a sensitivity analysis to find the best values for the surface temperature and CO yield that match experimental measurements. Afterward, validated smouldering properties are applied to construct the smouldering fire scenario in a large building open space (i.e., atrium) which is most common in the PBD. The simulated profiles of CO concentration from smouldering fire are analysed to calculate the ASET. Finally, smouldering fire scenarios are compared with the typical flaming fire scenarios that have the same fuel mass burning rate.

3.1. Model validation by full-scale smouldering fire tests

These two full-scale smouldering fire experiments [17,19] are chosen for the model validation. The detailed test information is summarised in Table 1. Both experiments were conducted in enclosure rooms. All external doors were closed, but the door gaps were not sealed. For the single-room model, the room size is 2.5 m high and 9 m^2 in floor area, and its layout is shown in Fig. 3a. Two small gaps of approximately 0.01 m^2, which imitate door gaps, are located at the top and bottom of the front face of the room. A sofa chair consists of a hardwood frame, cotton and polyurethane pads, and a polyurethane seat cushion, all covered with cotton fabric, which is placed at the centre of the room. It is assumed that it is a polyurethane foam fire.

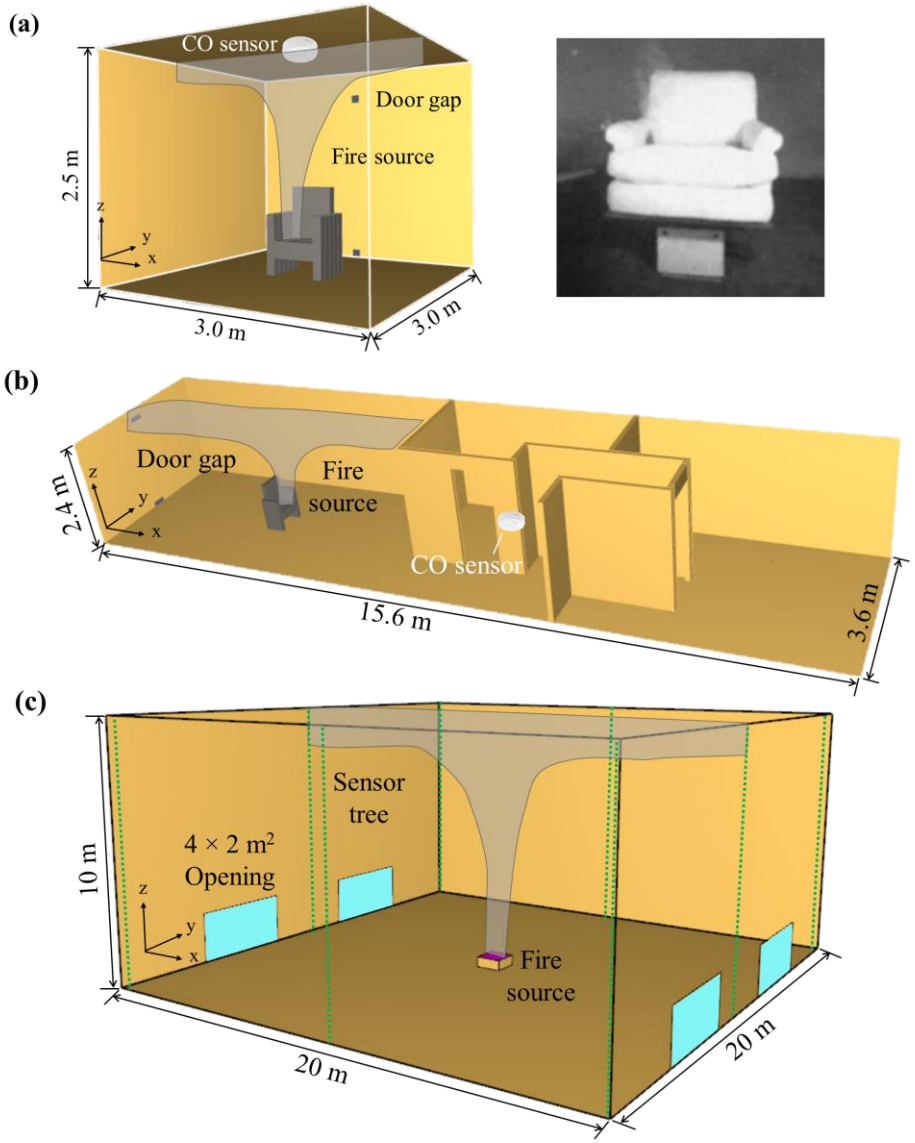

Fig. 3. Layout of (a) the single room test [19]; (b) the apartment test [17]; and (c) the large atrium.

Fig. 3a shows a picture from the full-scale experiment of a smouldering chair. The ignition starts from the left corner of the chair with a 0.1 × 0.1 m^2 surface which is 0.4 m above the floor level. The smouldering mass-loss rate of the chair was measured in the experiment [19] and fitted as

$$\dot{m} = \begin{cases} (0.10\ \text{g min}^{-2})t + (0.0185\ \text{g min}^{-3})t^2, & 0 < t < 60\ \text{min} \\ 73\ \text{g min}^{-1}, & 60 \leq t \leq 120\ \text{min} \end{cases} \quad (1)$$

which gives a peak smouldering mass-loss rate of 73 g/min (1.2 g/s) in the steady burning stage. A CO sensor is set at the centre of the ceiling of the room to measure and record the CO concentration. The cell size is determined by conducting a cell size sensitivity analysis (see Section 3.3). The simulation time is 7,200 s (120 min). The simulated CO concentration profile is compared to the result obtained from the full-scale experiment [19].

The apartment-home model consists of a living room, a rear room, a kitchen, and a hallway, as shown in Fig. 3b. The dimension of the apartment is 15.6 (length) × 3.6 (width) × 2.4 (height) m^3. The rear room and the kitchen are separated by partition walls with a thickness of 0.1 m. Two internal doors are opened, and the dimension of the doors is 0.8 (length) × 0.1 (width) × 2 (height) m^3. There are two door gaps located at the top and bottom of the living room wall, which is approximately 0.03 m^2 area. The smouldering chair is placed at the centre of the living room. This smouldering source has the same experimental setup as the single room test, ignition height, and smouldering mass-loss rate. Since we only focus on the CO concentration result, the emitted products are simplified to be only CO and CO_2. The specific CO yield is determined by later sensitivity analysis. One CO sensor is installed which is located in the middle of the hallway with a height of 1.5 m. The simulation time is 4,800 s or 80 min, and simulation results are compared to the experimental value by Bukowski [17].

Table 1. The computational setting for the numerical models, where soot yield is not set for smouldering to avoid confusion.

Parameters	**Single room** [19]	**Apartment** [17]	**Atrium**	
	Smouldering		**Smouldering**	**Flaming**
Floor area (m^2)	3 × 3	15.6 × 3.6	20 × 20	
Ceiling height (m)	2.5	2.4	5 – 10	
Door gaps (m^2)	Total 0.02	Total 0.06	Total 32	
Simulation time (s)	7,200	4,800	1,200	
Size of fire source	0.1 × 0.1 m^2 square		1 × 1 m^2 square	
Ignition height (m)	0.4 m above the ground		0.4 m above the ground	
Peak mass loss rate (g/s)	1.2		56 – 222	
Burning surface temp. (°C)	100 – 400		140	300 [29]
CO yield (g/g)	0.1 – 0.25		0.15	0.04 [30]
CO_2 yield (g/g)	0.75 – 0.9		0.85	1.84
Soot yield (g/g)	0		0	0.043 [31,32]

To calibrate the numerical model, sensitivity studies have been performed with the smouldering temperatures of 100°C to 400°C and the CO yield of 0.1 g/g to 0.25 g/g for both models. The ambient temperature in all simulations is set to 20°C. The numerical models are built by using Fire Dynamics Simulator (FDS) version 6.7.4 [33]. The default settings of the FDS are used, and any change of the default settings will be specified below.

3.2. Atrium smouldering fire model

Atrium, as one of the most commonly seen PBD practices, is selected to evaluate the hazard level of smouldering fires. A typical dimension of the atrium is predefined as 20 (length) × 20 (width) × 10 (height) m^3. Four-door openings with 4 × 2 m^2 are set at the floor level to allow natural air makeup. A 1 × 1 m^2 smouldering surface is placed at the centre of the atrium, as shown in Fig. 3c. The validated surface temperature and the CO properties from previous room-level models are applied in this model. Three peak fuel-burning mass-loss rates are modelled for different fire severities: 56, 111, and 222 g/s. Note that most of the heat production in smouldering is absorbed in the solid phase, rather than released to the gas plume, so it is inappropriate or misleading to use the HRR to describe a smouldering fire.

For a typical flaming fire on wood, a burning rate of 56 g/s will lead to an HRR = 0.056 kg/s × 18 MJ/kg = 1 MW, where 18 MJ/kg is the heat of combustion [34]. Similarly, the burning rates of 111 g/s and 222 g/s for flaming wood fire will lead to HRRs of 2 MW and 4 MW, respectively. Then, the smouldering and flaming fires can be compared under the same fuel-burning rate. As a common practice of PBD, the burning mass loss rates are conservatively set to reach the peak value at 300 s with a t-squared ramp-up curve.

It is generally considered that smouldering fires usually have a smaller burning mass loss rate in comparison to flaming fires. However, in some fire accidents (Fig. 1), smouldering fires could reach a high burning mass loss rate. Most flaming fires are caused by smouldering fires, and after the flame is extinguished, smouldering combustion could dominate the residual burning. Smouldering fires could not only reach a high burning rate but also release much more CO and other toxic gases, so they should be considered in addition to flaming fire scenarios.

The tenability limit of 800 ppm is selected for the CO concentration in this work [9], while the smoke-clearance height is set as 2 m, refer to [35]. The toxic gas will accumulate at the ceiling through the smoke plume first. Then, the gas layer will start to decrease along the walls due to boundary-layer flow and low gas temperature. Due to this behaviour, the CO sensor trees are set in the middle of each wall and corner to record the CO concentration descending profile with a spacing of 0.2 m. All results are obtained from the average value of the CO sensors trees near the corners. Also, 2D and 3D slices are set to record the gas flow pattern of the space. The flaming fire scenarios with the same mass loss rate of fuel burning defined by 10-m visibility are also explored, and then compared with smouldering fire under the same atrium design condition.

3.3. Sensitivity analysis of cell size

A sensitivity analysis is performed to investigate which cell size is suitable to simulate the smouldering process. After modelling the smouldering fire in the single room (Fig. 3a), we can get the velocity and CO concentration profiles. The velocity and CO sensors located in the middle of the room at a height of 1.6 m measure the smoke plume fluid velocity and CO concentration, respectively.

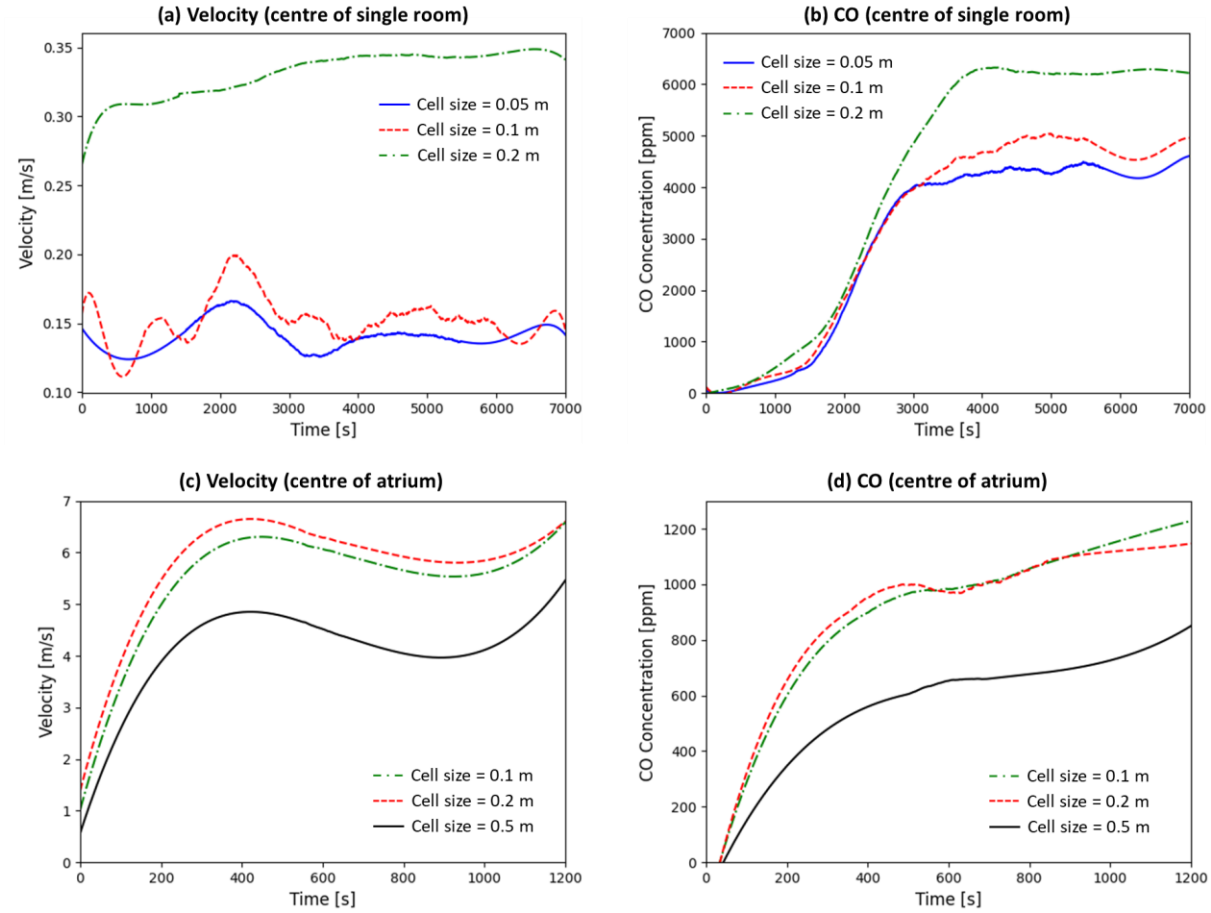

Fig. 4. Sensitivity analysis of cell size for room fire tests (a) velocity profiles, (b) CO profiles, and for modelling atrium (c) velocity profiles; and (d) CO profiles.

Fig. 4a illustrates that the fluid velocity of the smoke plume is insensitive to the 0.05 m and 0.1 m cell sizes since the corresponding curves are performed in a small discrepancy, while 0.2 m cell sizes have an obvious difference from the 0.05 m and 0.1 m cell sizes. As for CO concentration, although the profiles at the initial 2,500 s are very similar, there is a clear difference from the 0.2 m cell size result at a later stage (Fig. 4b). Therefore, cell sizes of 0.05 m and 0.1 m are capable of simulating the smouldering process. Then, a cell size of 0.1 m is adopted for the remaining simulations to save computational costs.

Additional sensitivity analysis of cell size (0.1 m, 0.2 m, and 0.5 m) is also performed for the atrium model because the burning mass-loss rate is larger than the room-level experiments. The velocity and CO concentration measurements are in the middle of the atrium. Fig. 4(c-d) shows that the cell sizes of

0.1 m and 0.2 m are insensitive to measure the velocity and CO concentration in this location, while the 0.5-m cell gives very different results. Therefore, 0.1 m and 0.2 m cell sizes can accurately simulate smouldering and flaming scenarios in the atrium model. To reduce the computational time and cost, a 0.2 m cell size is adopted for all atrium model simulations.

4. Validation Results

4.1. Smouldering Yield of Carbon Monoxide

Fig. 5 shows the simulated CO concentration results in the rooms for CO yields ranging from 0.1 g/g to 0.25 g/g, which are compared with experimental measurements in [19]. The surface temperature is preliminarily set as 140°C, which is based on the parametric study results and is discussed more in the next section.

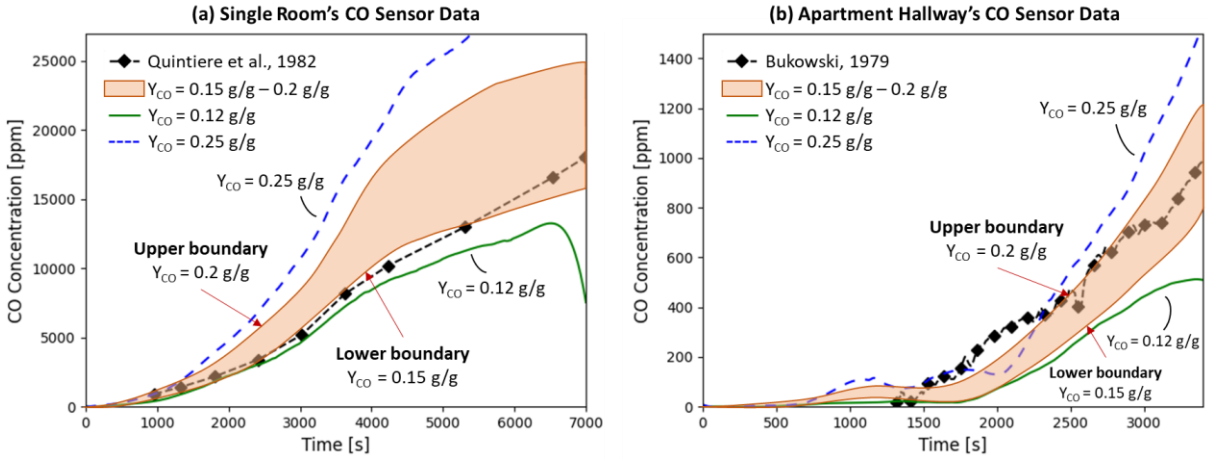

Fig. 5. Comparison between experimental and simulated CO profiles with a 140°C burning surface and different CO yields for (a) single room smouldering test; and (b) apartment smouldering test.

For the single room experiment (Fig. 5a), when the CO yield is below 0.15 g/g, the measured CO concentration at the ceiling CO sensor rises to 13,000 ppm before 6,500 s, which matches the experimental data well for the whole test period. At 7,000 s, the peak CO concentrations are 15,000 ppm (yield of 0.15 g/g) and 23,000 ppm (yield of 0.2 g/g), between which is the experimental value of 18,000 ppm. For modelling the apartment experiment (Fig. 5b), setting the CO yield between 0.15 g/g and 0.2 g/g, the modelled CO concentration also agrees well with the experimental data. For setting the lower CO yield of 0.12 g/g and a higher CO yield of 0.25 g/g in both cases, the modelling results become very different from the tests.

In short, numerical results with CO yield ranging from 0.15 g/g to 0.2 g/g agrees well with both single-room and apartment tests, and this range also agrees with other smouldering experiments in literature [36–41]. Therefore, a CO yield of 0.15 g/g is applied to the surface temperature validation and atrium smouldering fire simulations.

4.2. Characteristic Temperature of Smouldering Surface

According to our lab measurement of smouldering fire (Appendix A) and literature [36–41], the gas-plume temperature of smouldering emission is lower than 250°C, although the peak smouldering temperature inside the solid could reach 400-700°C. Then, a parametric study is performed with several surface temperatures, which range between 100°C and 400°C. The simulation results of the CO concentration in the models are shown in Fig. 6 for different surface temperatures. The CO yield is set to 0.15 g/g, as suggested in Section 4.1.

For the single room experiment (Fig. 6a), if the surface temperature is lower than 140°C, the measured CO concentration at the centre of the ceiling remains a 600 ppm until the end of the simulation, which is much lower than the experimental result. It is because the upward thermal buoyancy force due to the temperature difference between gases and ambient air is not large enough, thus the gas accumulates at the ground and leaks at a constant flow rate through the bottom door gap. When the temperature is between 140°C and 200°C, the CO concentration at the centre of the ceiling emerges with an increasing tendency. The peak values of CO concentration in this temperature range from 15,000 ppm to 19,000 ppm, which are close to the 18,000 ppm in the experiment. In this temperature range, both the increasing tendency and the peak values agree with the experiment. Although the CO concentration profiles with surface temperatures between 200°C and 400°C are similar to the experimental data during the first 5,300 s, the peak values at the end of the simulation are significantly lower than the measured ones. Note that the smouldering fire is an incomplete combustion phenomenon, and its burning temperature is much lower than ~1500°C of flaming fires [25,26].

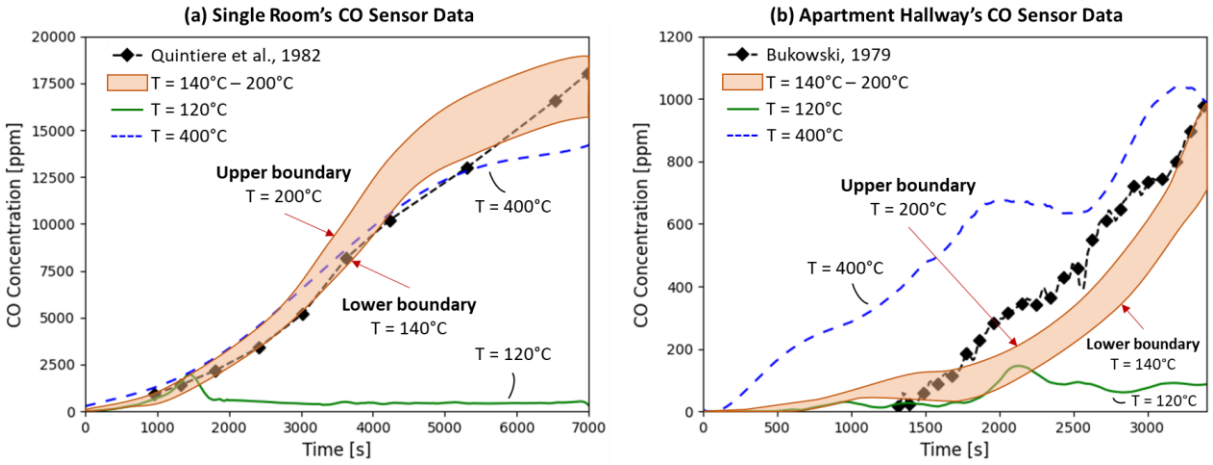

Fig. 6. Comparison between test and simulated CO levels with a CO yield of 0.15 and different surface temperatures for (a) single room smouldering test; and (b) apartment smouldering test.

For the apartment experiment (Fig. 6b), when the surface temperature is lower than 140°C, the CO concentration in the hallway could not reach 150 ppm. For the surface temperature between 140°C and 200°C, all the curves have an uptrend and have a peak CO concentration of 700-900 ppm in the hallway, agreeing with the measured peak value of 900 ppm. With a 400°C surface temperature, although the

peak CO concentration is close to the test result, the profile is significantly higher during the development stage.

To sum up, the numerical model with a surface temperature between 140°C and 200°C could provide similar CO concentration results to the measurements in both single-room and apartment experiments. Thus, together with the literature [36] and lab experiments, we choose a CO yield of 0.15 g/g and a surface temperature of 140°C for modelling smouldering fuel. Note that the CO yield and the surface temperature of the surrogate model are rough engineering analyses. Although the simulations with validated CO yield and surface temperature could match the room-scale experiments, they may not fully represent the real fire scenarios.

5. Smouldering Fire in Atrium

5.1. Base fire scenario in the atrium

With the validated model settings, a base scenario of smouldering fire is built in a 20 (length) × 20 (width) × 10 (height) m^3 atrium to identify the smouldering fire hazards in terms of CO concentration. The peak fuel burning mass-loss rate is firstly set as 56 g/s, which is reached at 300 s under t squared law for simplicity. For this based case, the ASET defined by the maximum CO concentration of 800 ppm at 2-m height is around 359 s (Table 2 and Fig. 7a).

A flaming fire with the same burning rate is also analysed, where its ASET is defined by a 10-m visibility limit, which is a common practice in current PBD. Fig. 7 shows very similar ASETs for the flaming fire (10-m visibility) and smouldering fire (800-ppm CO) under the same fuel-burning rate. However, the evolutions of these two tenability profiles are very different. Using the base case (a burning rate of 56 g/s in Fig. 7a) as the example, the CO concentration profile of smouldering fire starts to drop at around 320 s with a very rapid and stable speed. In contrast, the 10-m visibility profile of a flaming fire drops much earlier at about 160 s, and its initial drop speed is much faster up to about 6-m height. Afterward, its drop speed becomes much slower than that for smouldering. Overall, the 10-m visibility profile of flame reaches 2 m at 339 s, which is 20 s less than smouldering fire.

Table 2. Comparing available safe egress time (ASET) between smouldering and flaming fires under the same fuel-burning mass-loss rate (MLR) under different fire sizes and atrium heights.

Atrium Height	56 g/s burning rate		111 g/s burning rate		222 g/s burning rate	
	Smouldering (800 ppm CO)	1-MW Flaming (10-m visibility)	Smouldering (800 ppm CO)	2-MW Flaming (10-m visibility)	Smouldering (800 ppm CO)	4-MW Flaming (10-m visibility)
5 m	294 s	262 s	224 s	210 s	184 s	170 s
10 m (Base)	359 s	339 s	296 s	283 s	238 s	225 s
15 m	425 s	406 s	342 s	322 s	273 s	265 s
20 m	504 s	437 s	376 s	344 s	314 s	271 s

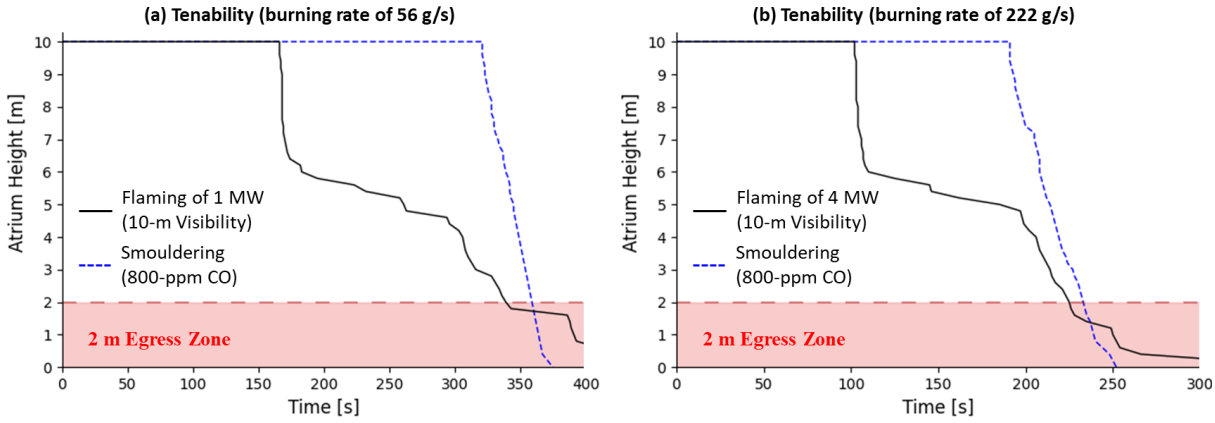

Fig. 7. The tenability profiles for the fires with (a) 56 g/s MLR or 1 MW HRR; and (b) 222 g/s MLR or 4 MW HRR, while the solid lines are the 10-m visibility profile from flaming fires and dashed lines are the 800 ppm CO concentration profile from smouldering fires.

Fig. 8a further illustrates the simulated CO transport inside the atrium of the base-case smouldering fire (see Video S1). At the early stage of a smouldering fire, the gas temperature above the fire source was still high enough (i.e., 140°C) to create a buoyant plume (imaging the cigarette smoke). The buoyancy force drives the hot CO emission to flow upward and reach the ceiling at about 130 s. By mixing with the cold ambient air, the fire emission temperature on the ceiling approaches the ambient temperature, so the buoyancy force becomes too small to form a thick hot layer. This is different from the much hotter emission from the flaming fire (see Fig. 8b), where a thick and stable hot smoke layer will be first formed below the ceiling.

Afterward, the smouldering CO emission moves downwards along the walls, driven by its initial momentum (or the inertia), forming a thin boundary layer and reaching the floor at about 350 s. Therefore, the 800 ppm CO threshold drops very quickly at that moment, as shown in Fig. 7. Note that the formed CO boundary-layer flow does not stop on the floor at 420 s, but it continues travelling and mixing on the floor. Quickly, a highly toxic layer of high-concentration of CO is formed right above the ground, all occupants and rescue personnel would expose to a lethal environment. Unlike the flaming fire, the smouldering fire is not able to form a two-zone model (i.e., hot upper zone and the cold lower zone) because of much lower smoke and burning temperature and weakter buoyancy force. Moreover, it is worth noting that although masks can block some smoke particles, no mask can prevent the infiltration of CO.

Fig. 8b shows the smoke flow of the flaming fire for comparison, denoted by the 10-visibility profile. Different from the smouldering fire, the smoke layer from hot flame accumulates beneath the ceiling rather than sliding down along the walls and forms a two-zone model, because the hotter smoke layer is pushed by a larger buoyancy force. The smoke layer only moves downward because of the volume expansion. When the smoke layer approaches the ground, the cold inlet airflow from opening

also prevents the smoke from further descending. Then, even after the 10-m visibility reaches the height of 2 m above the ground, most of the near-ground area still has high visibility.

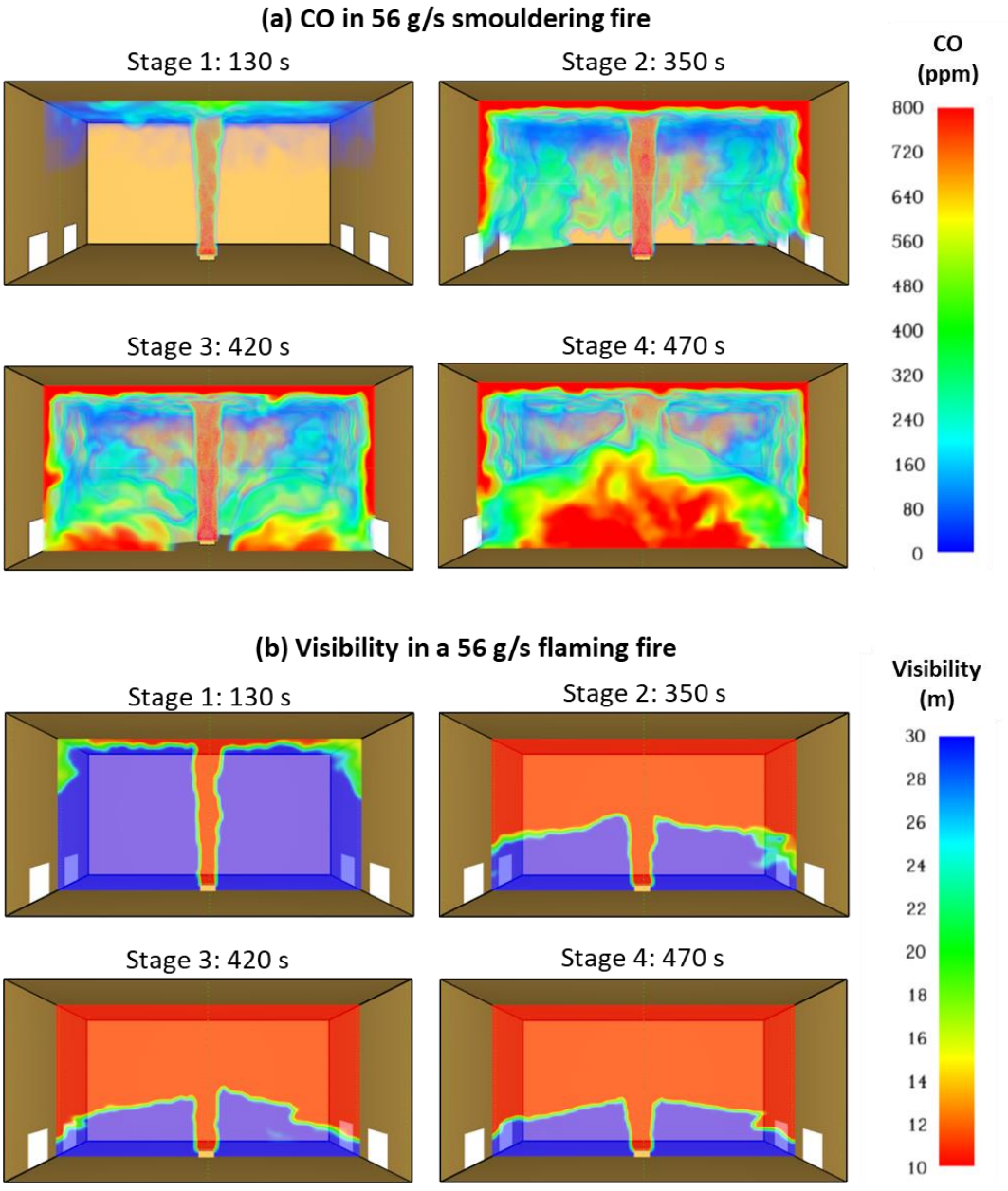

Fig. 8. For the same burning mass-loss rate of 56 g/s, (a) simulated smouldering fire gas movement and development; and (b) 1-MW flaming fire soot distribution (see Video S1).

To ensure the fidelity of the above findings, tenability profile comparisons between smouldering and flaming fires have been performed with fuel-burning mass loss rates of 111 g/s and 222 g/s (see Fig. 7b). The difference in ASET between flaming and smouldering is also fairly close. Therefore, despite a similar ASET for the smouldering and flaming fire scenarios, the post-limit fire environments are very different. In flaming fire, the smoke layer tends to maintain at certain heights, while the near-ground zone is smoke-free due to the opening. In the smouldering fire, however, the CO and other toxic gases accumulate on the ground floor, which is a significant threat to occupants and fire rescue teams.

5.2. Influence factors for smouldering CO hazards

Building fire safety is affected by many factors, e.g., architectural design, fire protection provision, and fire scenarios. This section explores how different building and fire features affect the hazardous level of the smouldering fire and its CO emission.

Atrium height. The atrium heights of 5 m, 10 m, 15 m, and 20 m are investigated to see how the height affects the fire safety level of both smouldering and flaming fires. The ASET results for all fire scenarios are also summarised in Table 3, and their tenability descending profile are compared in Fig. 9a. As expected, a higher atrium can create a larger ASET value because it takes a longer time for fire smoke to move up and down (see Video S2).

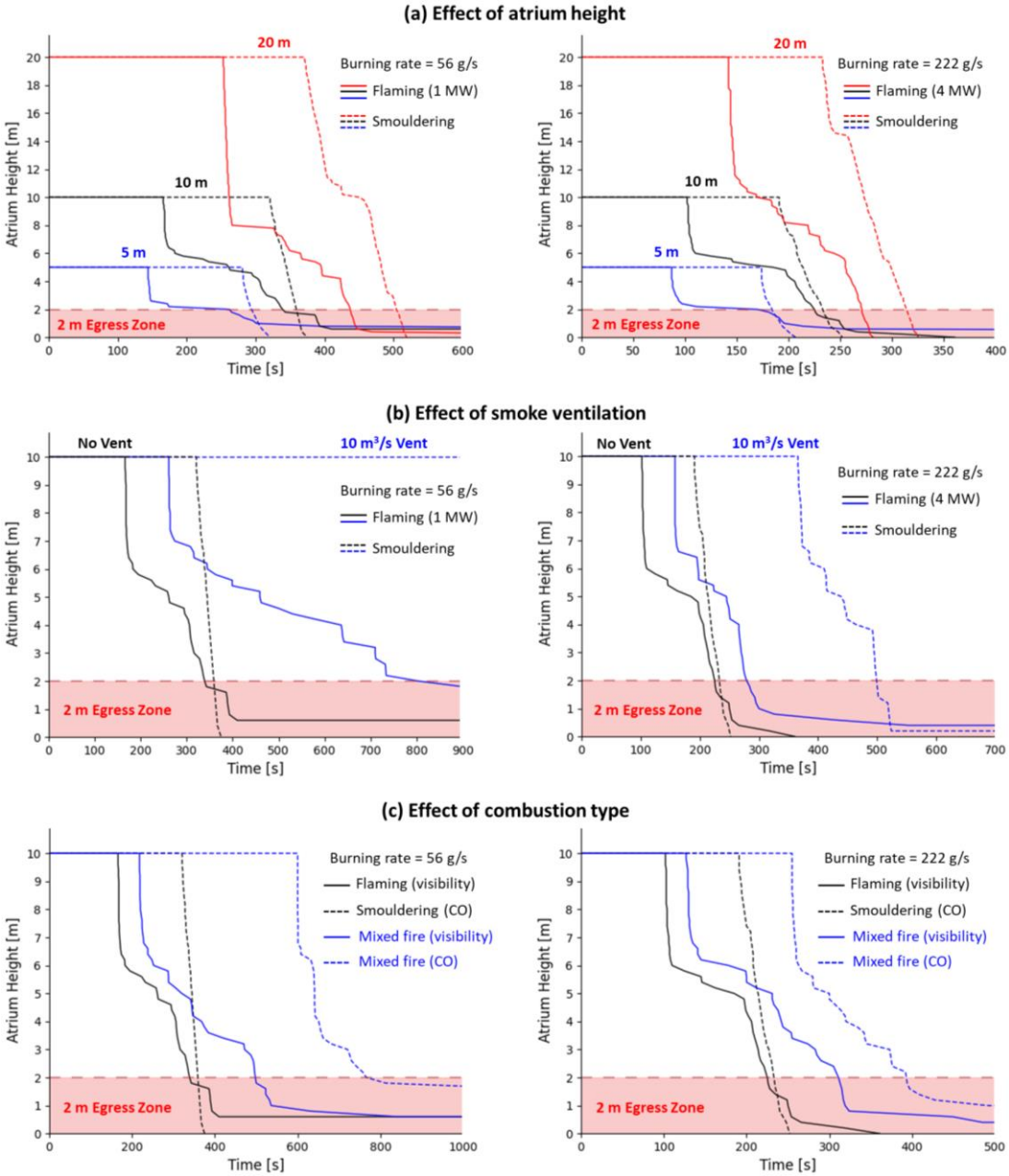

Fig. 9. The effect of (a) atrium height; (b) ventilation; and (c) combustion type on the tenability profiles for fires with three different fire sizes

More importantly, the 800-ppm CO from the smouldering fire can reach the 2-m height at a similar time as the 10-m visibility from the flaming fire, showing a similar ASET. The difference between flaming and smouldering decreases with atrium height. In addition, we can see all CO-concentration curves drop very smoothly and at a similar descending speed. It means the driven force for CO emission is the same, and a similar boundary flow on the wall (see Fig. 8a) is formed, independent of atrium height and burning rate.

Smoke ventilation system. A smoke ventilation system is a widely used fire safety provision in the atrium. Then, the effect of the mechanical ventilation system on CO emission from the smouldering fire is investigated. Fig. 9b compares the smoke descending profiles with and without ventilation (see Video S3). For a flaming fire burning at 56 g/s, a 10 m^3/s smoke extraction system can increase the ASET from 339 s to 804 s. For a smouldering fire of the same burning rate, the ventilation system is even more effective, which allows the atrium to maintain a tenable condition for more than 1200 s. This is mainly because the cooler smouldering fire only induces a weaker-buoyancy plume that has a lower smoke mass flow rate. Then, the CO emission is more easily extracted from the space, compared to the larger smoke-induced by the stronger plume from the hot flame.

With the increase of the fire size, the improvement of the ASET by the ventilation system becomes smaller. For 222 g/s MLR fire scenarios, the ventilation system can only increase the ASET by 24% in a flaming fire situation, while for a smouldering fire, it can still double its ASET. Hence, the ventilation system is particularly effective for smouldering fires, even with large fire sizes.

Type of combustion/fire. In realistic fire scenarios, flaming and smouldering fires both exist in the burning of different fuels and at different burning stages. Both flaming and smouldering can produce opaque smoke, CO, and other toxic gases. Their smoke emissions are also mixed in the plume and smoke layer, so it is impossible to separate them from the fire source. For simplicity, we consider a mixed fire with half of the fuel burnt in flaming and the other burnt in smouldering. Using the base case (total fuel-burning rate of 56 g/s) as an example, 28 g/s is burnt in flame to generate an HRR of 0.5 MW and the other 28 g/s is burnt in smouldering.

Table 3. Comparing available safe egress time (ASET) between smouldering and flaming fires of the same fuel-burning mass-loss rate (MLR) inside a 10-m atrium under different design features.

Fire and vent Scenarios	**56 g/s MLR (Base case)**		**111 g/s MLR**		**222 g/s MLR**	
	Smouldering (800 ppm CO)	1-MW Flaming (10-m visibility)	Smouldering (800 ppm CO)	2-MW Flaming (10-m visibility)	Smouldering (800 ppm CO)	4-MW Flaming (10-m visibility)
10 m^3/s vent	>1,200 s	804 s	>1,200 s	361 s	499 s	279 s
No vent	359 s	339 s	269 s	283 s	238 s	225 s
	742 s (CO), 498 s (Visibility) Half smoulder & half flame		517 s (CO), 364 s (Visibility) Half smoulder & half flame		393 s (CO), 311 s (Visibility) Half smoulder & half flame	

Fig. 9c compares the tenability profiles of different combustion types (see Video S4). It can be seen that in the mixed fire scenarios, the 10-m smoke visibility still reaches the tenability limit quicker than the 800-ppm CO concentration. Although the combination fires present both hazards from soot and CO productions, the overall safety level would be higher than the single-type combustion scenarios of the same fuel burning rate in terms of ASET. There are two reasons. Firstly, the ASET is defined by the first criteria exceeding the tenability limit, where smouldering and flaming do not help each other to reach their limit. Secondly, the flaming fire can induce a much stronger smoke plume and dominate the smoke transport. Then, the CO from smouldering will follow the flaming plume to accumulate below the ceiling rather than form a descending boundary-layer flow on the wall.

Therefore, the mixed flaming-and-smouldering fire scenario is not necessarily a conservative design scenario. During the performance-based design of building fire safety, the CO hazard in the smouldering fire and the visibility drop in the flaming fire should be considered separately. Not only should engineers find the fire scenarios showing the smallest ASET, but we also should consider the overall fire hazardous level after the threshold tenability condition is breached.

Future work should consider different burning curves, based on fuel smouldering characteristics. Simulations of multiple smouldering sources, various fire sizes, and building features (e.g., opening factor, HVAC system, layout) are also needed to investigate their influence on the smouldering hazardous level and the building fire safety performance. By considering these smouldering fire scenarios, we can improve the overall fire safety margin, understand the true fire hazard better, and support the fire evacuation and rescue processes.

6. Conclusions

This work investigates the smouldering fire scenarios and their CO hazards in assessing the fire safety performance of the building. By reproducing the two full-scale fire experiments, we found the CO yield of 0.15-0.2 g/g and the fuel surface temperature of 140-200°C as the boundary condition can accurately simulate the smouldering fire source. These properties could provide valuable contributions to the rough engineering analysis aimed at predicting CO emissions from a smouldering fire.

Modelling of atrium fires shows that the ASETs of smouldering fires, defined by the CO concentration of 800 ppm, are comparable to the values of flaming fires, defined by the 10-m smoke visibility. However, the building environment with a smouldering fire presents a greater threat to the occupants and rescue teams, because a high concentration of CO and other toxic gases accumulate on the ground level. Hence, scenarios and hazards of smouldering fire shall not be ignored during the performance-based design process.

Simulations further reveal that by decreasing the atrium height, the difference in ASET between smouldering and flaming fires becomes smaller. The ceiling mechanical smoke ventilation system is more effective in extracting CO and reducing the hazard of smouldering fires. Moreover, a mixed fire

scenario with half smouldering and half flaming shows a larger ASET, so it is not necessarily the worst design-fire scenario.

In performance-based fire safety design, the CO hazard from the smouldering fires and the visibility limit in flaming fires should be taken into account separately. Although the smallest ASET of the fire scenarios implies the tenability limit of the building, the consideration of the CO hazard of smouldering fire is also important to discover the overall fire hazard level of the building. Future research should consider smouldering fire in other building scenarios (e.g., tunnel and underground space) with different fire scenarios and design features.

Acknowledgement

This work is funded by the Hong Kong Research Grants Council Theme-based Research Scheme (T22-505/19-N).

Supplementary Materials

Link to access the Supplementary Videos

Appendix

A lab experiment has been performed to verify the surface temperature of the FDS models. The experiment setup is shown in Fig. A1(a), where a smouldering cotton was ignited by a heating coil. Three thermocouples were touching the top surface of the smouldering cotton that could measure the true fuel surface temperature (as well as the initial emission temperature) when smouldering fire is burning internally. Fig. A1(b) shows the evolution of measured surface temperatures. Specifically, the peak surface temperature of smouldering cotton is less than 250°C, and the average smouldering gas temperature is 140 ± 20°C. Therefore, it is reasonable to set the surface temperature to 140°C for modelling a typical smouldering fire.

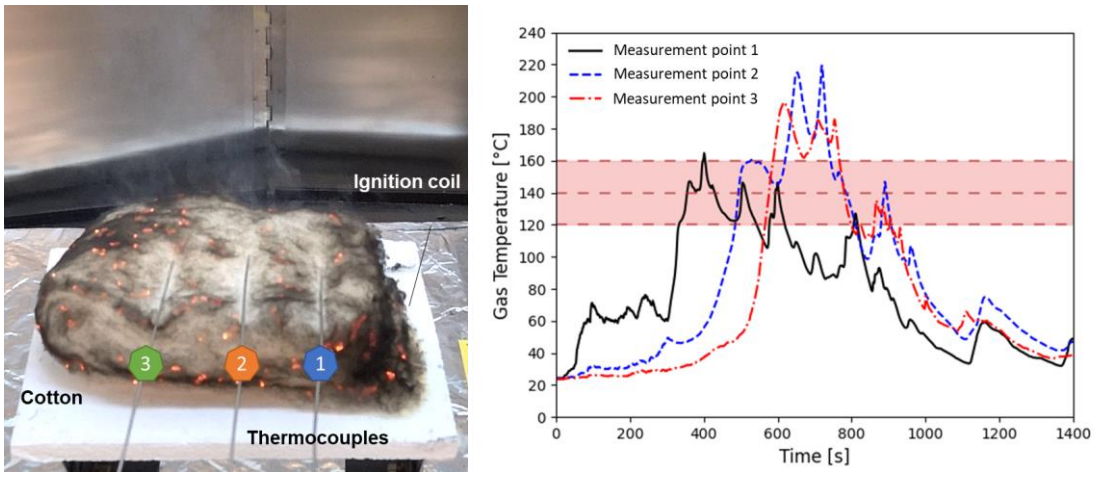

Fig. A1. (a) Experiment for measuring the cotton smouldering gas temperature; and (b) measured smouldering gas temperature profiles in 3 measurement points.

References

[1] A.A. Stec, Fire toxicity – The elephant in the room?, Fire Safety Journal. 91 (2017) 79–90. https://doi.org/10.1016/j.firesaf.2017.05.003.

[2] Fire statistics data tables - GOV.UK, (n.d.).

[3] W.M. Pitts, The global equivalence ratio concept and the formation mechanisms of carbon monoxide in enclosure fires, Progress in Energy and Combustion Science. 21 (1995) 197–237. https://doi.org/10.1016/0360-1285(95)00004-2.

[4] D.A. Purser, J.L. McAllister, Assessment of Hazards to Occupants from Smoke, Toxic Gases, and Heat, SFPE Handbook of Fire Protection Engineering, Fifth Edition. (2016) 2308–2428. https://doi.org/10.1007/978-1-4939-2565-0_63.

[5] C.W. Runyan, R.M. Johnson, J. Yang, A.E. Waller, D. Perkis, S.W. Marshall, T. Coyne-Beasley, K.S. McGee, Risk and protective factors for fires, burns, and carbon monoxide poisoning in U.S. households, American Journal of Preventive Medicine. 28 (2005) 102–108. https://doi.org/10.1016/j.amepre.2004.09.014.

[6] M. Kohno, T. Okazaki, Performance Based Fire Engineering in Japan, International Journal of High-Rise Buildings. 2 (2013) 23–30. https://doi.org/10.21022/IJHRB.2013.2.1.023.

[7] S.C. Tsui, Performance-Based Fire Safety Design in Hong Kong, International Journal on Engineering Performance-Based Fire Codes. 6 (2004) 223–229.

[8] B.S. Institution, BS 7974:2019 Application of Fire Safety Engineering Principles to the Design of Buildings - Code of Practice, British Standards Institution. 1 (2019) 7–68.

[9] PD 7974-6:2019 | 31 Mar 2019 | BSI Knowledge, (n.d.).

[10] L.H. Hu, N.K. Fong, L.Z. Yang, W.K. Chow, Y.Z. Li, R. Huo, Modeling fire-induced smoke spread and carbon monoxide transportation in a long channel: Fire Dynamics Simulator comparisons with measured data, Journal of Hazardous Materials. 140 (2007) 293–298. https://doi.org/10.1016/j.jhazmat.2006.08.075.

[11] D. Yang, R. Huo, X.L. Zhang, S. Zhu, X.Y. Zhao, Comparative study on carbon monoxide stratification and thermal stratification in a horizontal channel fire, Building and Environment. 49 (2012) 1–8. https://doi.org/10.1016/j.buildenv.2011.09.009.

[12] US Fire Administration, Fire-Related Firefighter Injuries Reported to the National Fire Incident Reporting System (2015-2017), Topical Fire Report Series. 20 (2019) 15.

[13] R.L. Alpert, Turbulent ceiling-jet induced by large-scale fires, Combustion Science and Technology. 11 (1975) 197–213. https://doi.org/10.1080/00102207508946699.

[14] Y. Zeng, H.Y. Wong, W. Węgrzyński, X. Huang, Revisiting Alpert's Correlations: Numerical Exploration of Early-Stage Building Fire and Detection, Fire Technology. (2023). https://doi.org/10.1007/s10694-023-01461-0.

[15] A. Khan, T. Zhang, X. Huang, A. Usmani, Machine Learning Driven Smart Fire Safety Design

of False Ceiling and Emergency Machine, Process Safety and Environmental Protection (under Review). 177 (2023) 1294–1306. https://doi.org/10.1016/j.psep.2023.07.068.

[16] R. Bukowski, T.E. Waterman, W.J. Christian, Center for Fire Research (U.S.), Detector sensitivity and siting requirements for dwellings, (1977) 370.

[17] R.W. Bukowski, Investigation of the Effects of Heating and Air Conditioning on the Performance of Smoke Detectors in Mobile Home. Final Report., (1979).

[18] G. Heskestad, Escape potentials from apartments protected by fire detectors in high-rise buildings, Factory Mutual Research, Norwood Mass., 1974.

[19] J.G. Quintiere, M. Birky, F. Macdonald, G. Smith, An analysis of smoldering fires in closed compartments and their hazard due to carbon monoxide, Fire and Materials. 6 (1982) 99–110. https://doi.org/10.1002/fam.810060302.

[20] Y. Hu, N. Fernandez-Anez, T.E.L.L. Smith, G. Rein, Review of emissions from smouldering peat fires and their contribution to regional haze episodes, International Journal of Wildland Fire. 27 (2018) 293–312. https://doi.org/10.1071/WF17084.

[21] G. Rein, S. Cohen, A. Simeoni, Carbon emissions from smouldering peat in shallow and strong fronts, Proceedings of the Combustion Institute. 32 (2009) 2489–2496. https://doi.org/10.1016/j.proci.2008.07.008.

[22] Y. Chen, S. Lin, Z. Liang, N.C. Surawski, X. Huang, Smouldering organic waste removal technology with smoke emissions cleaned by self-sustained flame, Journal of Cleaner Production. 362 (2022). https://doi.org/10.1016/j.jclepro.2022.132363.

[23] M.S. Saidi, M.R. Hajaligol, A. Mhaisekar, M. Subbiah, A 3D modeling of static and forward smoldering combustion in a packed bed of materials, Applied Mathematical Modelling. 31 (2007) 1970–1996. https://doi.org/10.1016/J.APM.2006.08.003.

[24] D.A. Purser, Toxic Combustion Product Yields as a Function of Equivalence Ratio and Flame Retardants in Under-Ventilated Fires: Bench-Large-Scale Comparisons, Polymers. 8 (2016). https://doi.org/10.3390/POLYM8090330.

[25] T.J.T.J. Ohlemiller, Modeling of smoldering combustion propagation, Progress in Energy and Combustion Science. 11 (1985) 277–310. https://doi.org/10.1016/0360-1285(85)90004-8.

[26] G. Rein, Smoldering Combustion, SFPE Handbook of Fire Protection Engineering. 2014 (2014) 581–603. https://doi.org/10.1007/978-1-4939-2565-0_19.

[27] (PDF) Fire research report Smoke Alarms in Homes An Analysis, (n.d.).

[28] K. McGrattan, S. Hostikka, R. McDermott, J. Floyd, C. Weinschenk, K. Overholt, Sixth Edition Fire Dynamics Simulator Technical Reference Guide Volume 1 : Verification guide, 1 (2015) 1–147.

[29] K. Mcgrattan, S. Hostikka, R. Mcdermott, J. Floyd, C. Weinschenk, K. Overholt, Fire Dynamics Simulator User's Guide, (n.d.).

[30] C.M. Fleischmann, Is prescription the future of performance-based design?, Fire Safety Science.

(2011) 77–94. https://doi.org/10.3801/IAFSS.FSS.10-77.

[31] L.-C. Su, X. Wu, X. Zhang, X. Huang, Smart performance-based design for building fire safety: Prediction of smoke motion via AI, Journal of Building Engineering. 43 (2021) 102529. https://doi.org/10.1016/j.jobe.2021.102529.

[32] M.M. Khan, M. Chaos, Combustion characteristics of materials and generation of fire products, SFPE Handbook of Fire Protection Engineering, Fifth Edition. (2016) 1143–1232. https://doi.org/10.1007/978-1-4939-2565-0_36/FIGURES/27.

[33] K. McGrattan, S. Hostikka, R. McDermott, J. Floyd, C. Weinschenk, K. Overholt, FDS technical reference guide volume 1 : Mathematical Model, 2017. https://doi.org/10.6028/NIST.SP.1018-1.

[34] M.J. Hurley, D. Gottuk, J.R. Hall, K. Harada, E. Kuligowski, M. Puchovsky, J. Torero, Jj.M. Watts, C. Wieczorek, SFPE handbook of fire protection engineering, fifth edition, 2016. https://doi.org/10.1007/978-1-4939-2565-0.

[35] Hong Kong Government, Code of Practice for Fire Safety in Buildings, (2015) 1–234.

[36] X. Huang, G. Rein, Upward-and-downward spread of smoldering peat fire, Proceedings of the Combustion Institute. 37 (2019) 4025–4033. https://doi.org/10.1016/j.proci.2018.05.125.

[37] M. Malow, U. Krause, Smouldering combustion of solid bulk materials at different volume fractions of oxygen in the surrounding gas, Fire Safety Science. 9 (2008) 303–314. https://doi.org/10.3801/IAFSS.FSS.9-303.

[38] L. Shi, M.Y.L. Chew, Experimental study of carbon monoxide for woods under spontaneous ignition condition, Fuel. 102 (2012) 709–715. https://doi.org/10.1016/j.fuel.2012.06.053.

[39] H. Wang, P.J. van Eyk, P.R. Medwell, C.H. Birzer, Z.F. Tian, M. Possell, X. Huang, Smouldering fire and emission characteristics of Eucalyptus litter fuel, Fire and Materials. 46 (2022) 576–586. https://doi.org/10.1002/fam.3004.

[40] Z. Liang, S. Lin, X. Huang, Smoldering ignition and emission dynamics of wood under low irradiation, Fire and Materials. (2022) 1–11. https://doi.org/10.1002/fam.3107.

[41] A.A. Stec, T.R. Hull, Assessment of the fire toxicity of building insulation materials, Energy and Buildings. 43 (2011) 498–506. https://doi.org/10.1016/j.enbuild.2010.10.015.